Shape transformations of epithelial shells

Supporting Material

M. Misra, B. Audoly, I. G. Kevrekidis and S. Y. Shvartsman

S1: Numerical Aspects - 3D model

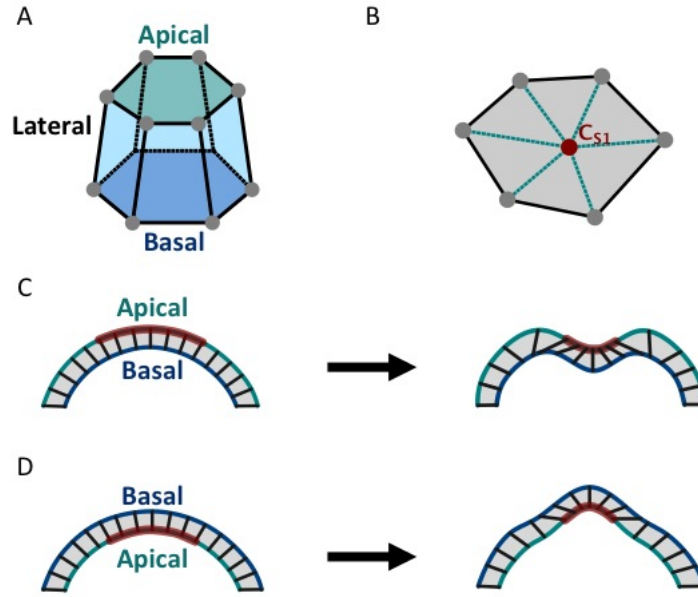## S1.1: Surface area, cell volume and inner-cavity volume

Figure S1: **(A)** Schematic representation of a 'lampshade' shaped 3D cell with distinct apical, basal, and lateral surfaces. **(B)** Schematic of a representative surface of a 3D cell showing triangular sub-elements as formed by surface nodes and surface centroid $\mathbf{C}_{S1}$. The surface area is defined as the sum of the areas of triangular sub-elements (discussed more in S1.1). **(C)** Schematic illustrating the *apical-out* case, where the apical side forms the *outer* surface of the epithelial shell. Apical constriction of a patch of cells leads to invagination. **(D)** Schematic illustrating the *apical-in* case, where the apical side forms the *inner* surface of the epithelial shell. Apical constriction of a patch of cells leads to evagination.

3D cells are modeled as 'lampshade' shaped prisms (Fig. S1(A)). Given the coordinates and specific ordering of vertices (which we will explain more later), we can define edges, surfaces, and the volume of the cell. In this section, we will describe how we define each of these geometric features for numerical implementation.

The length of an edge, as formed by two neighboring vertices $\mathbf{r}_{i+1}$ and $\mathbf{r}_i$, is

$$l_e = |\mathbf{r}_{i+1} - \mathbf{r}_i|, \tag{1}$$

1

where $\mathbf{r}_i = x_i\hat{\mathbf{i}} + y_i\hat{\mathbf{j}} + z_i\hat{\mathbf{k}}$.

The nodes that constitute a 'surface' ($\mathbf{r}_0, \mathbf{r}_1, ..., \mathbf{r}_{n-1}$ where n is the number of vertices in a surface) can be nonplanar. We build a surface from these nodes by defining triangular sub-elements (as formed by $\mathbf{r}_i$, $\mathbf{r}_{i+1}$ and $\mathbf{C}_{s1}$ and for $i \in [0, n-1]$, as shown in Fig. S1(B)). $\mathbf{C}_{s1}$ is the centroid of the surface, which is defined as mean position of the nodes belonging to the surface. The area of the surface A_{s1} is defined as the sum of the areas of traingular sub-elements in the following way

$$A_{s1} = \sum_{i=0}^{n-1}|\mathbf{A}_i|,$$

$$\mathbf{A}_i = \frac{1}{2}(\mathbf{r}_{i+1} - \mathbf{C}_{s1}) \times (\mathbf{r}_i - \mathbf{C}_{s1}), \tag{2}$$

$$\mathbf{C}_{s1} = \frac{1}{n}\sum_{i=0}^{n-1}\mathbf{r}_i.$$

We define the ordering of the vertices such that the surface area vector (as defined in Eq. 2) points in the 'outward' direction with respect to the cell.The volume of a cell is defined in the following way

$$V_c = \sum_{j=0}^{n_s-1}V_j,$$

$$V_j = \sum_{i=0}^{n-1}\frac{1}{3}\mathbf{A}_i \cdot \mathbf{C}_j, \tag{3}$$

where n_s is the number of surfaces in the cell, and V_j is the (signed) volume of a pyramids formed by triangular sub-elements of the surface j as the base and the reference origin as the apex. The volume of the cell V_c can be calculated by taking the sum of the (signed) volume V_j over all surfaces of the cell. $\mathbf{A}_i$ is the area vector associated with the triangular sub element i, and $\mathbf{C}_j$ is the centroid of surface j (as defined in Eq. 2).

We use similar ideas to calculate the volume of the inner cavity of the epithelial shell V_Y and is defined in the following way

$$V_Y = \sum_{k=0}^{N_b-1}V_k,$$

$$V_k = \sum_{i=0}^{n-1}\frac{1}{3}\mathbf{A}_i \cdot \mathbf{C}_k, \tag{4}$$

where N_b is the number of cell surfaces on the inner side of the shell. Note that the inner surface of the epithelial shell is formed by the apical side in the *apical-in* case and by the basal side in the *apical-out* case (see main text for details).

S1.2: Numerical implementation of the energy gradient

To find equilibrium shapes, we find configurations with zero net force. In this section, we will describe how we found analytical expressions for forces on each vertex. The net force on a vertex r_i is given as,

$$\mathbf{F}_i = -\nabla_i E = -(\frac{\partial E}{\partial \mathbf{x}_i}\hat{\mathbf{i}} + \frac{\partial E}{\partial \mathbf{y}_i}\hat{\mathbf{j}} + \frac{\partial E}{\partial \mathbf{z}_i}\hat{\mathbf{k}}). \tag{5}$$

This net force can be split into different terms corresponding to different energy contributions due to apical edges, lateral surfaces, basal surfaces, and due to the volume incompressibility term (eq. 1, main text).

The force on a vertex $\mathbf{r}_i$ due to an apical edge $e1$ is

$$E_{e1} = \sigma l_{e1} = \sigma|\mathbf{r}_{i+1} - \mathbf{r}_i|,$$
$$\mathbf{F}_{e1} = -\sigma\frac{\mathbf{r}_{i+1} - \mathbf{r}_i}{|\mathbf{r}_{i+1} - \mathbf{r}_i|}. \tag{6}$$

We get the net force due to apical edges on a given vertex by adding the contribution from all three adjacent apical edges.

The force on a vertex $\mathbf{r}_i$ due to a lateral surface $s1$ is

$$E_{s1} = \alpha A_{s1},$$
$$\mathbf{F}_{s1} = -\alpha\nabla_i A_{s1}. \tag{7}$$

Neighboring vertices of $\mathbf{r}_i$ in a surface $s1$ (as defined before) are $\mathbf{r}_{i+1}$ and $\mathbf{r}_{i-1}$. We identify two triangular sub-elements A_1 and A_2 which have contributions from $\mathbf{r}_i$.

$$A_{s1} = |\mathbf{A}_1| + |\mathbf{A}_2| + \sum_{\substack{j=0 \\ j \neq i,i+1}}^{n-1} |\mathbf{A}_j|, \tag{8}$$

where $\mathbf{A}_1 = \frac{1}{2}(\mathbf{r}_i - \mathbf{C}_{s1}) \times (\mathbf{r}_{i-1} - \mathbf{C}_{s1})$, $\mathbf{A}_2 = \frac{1}{2}(\mathbf{r}_{i+1} - \mathbf{C}_{s1}) \times (\mathbf{r}_i - \mathbf{C}_{s1})$, and $\mathbf{A}_j = \frac{1}{2}(\mathbf{r}_j - \mathbf{C}_{s1}) \times (\mathbf{r}_{j-1} - \mathbf{C}_{s1})$.

Next, we show the terms involved in the definition of the derivative of the surface area that are needed to calculate the surface force.

$$\nabla_i A_{s1} = \nabla_i|\mathbf{A}_1| + \nabla_i|\mathbf{A}_2| + \sum_{\substack{j=0 \\ j \neq i,i+1}}^{n-1} \nabla_i|\mathbf{A}_j|,$$
$$\mathbf{A}_{1,2,j} = A^x_{1,2,j}\hat{\mathbf{i}} + A^y_{1,2,j}\hat{\mathbf{j}} + A^z_{1,2,j}\hat{\mathbf{k}},$$

$$\nabla_i |\mathbf{A}_{1,2,j}| = \frac{1}{|\mathbf{A}_{1,2,j}|} \left(\left(A^x_{1,2,j} \frac{\partial A^x_{1,2,j}}{\partial x_i} + A^y_{1,2,j} \frac{\partial A^y_{1,2,j}}{\partial x_i} + A^z_{1,2,j} \frac{\partial A^z_{1,2,j}}{\partial x_i} \right) \hat{\mathbf{i}} \right.$$

$$+ \left(A^x_{1,2,j} \frac{\partial A^x_{1,2,j}}{\partial y_i} + A^y_{1,2,j} \frac{\partial A^y_{1,2,j}}{\partial y_i} + A^z_{1,2,j} \frac{\partial A^z_{1,2,j}}{\partial y_i} \right) \hat{\mathbf{j}}$$

$$\left. + \left(A^x_{1,2,j} \frac{\partial A^x_{1,2,j}}{\partial z_i} + A^y_{1,2,j} \frac{\partial A^y_{1,2,j}}{\partial z_i} + A^z_{1,2,j} \frac{\partial A^z_{1,2,j}}{\partial z_i} \right) \hat{\mathbf{k}} \right). \quad (9)$$

Using the definition for the area (Eq. 2) and simple algebraic manipulations, we get the expressions for the terms involved in the derivative of the surface area (Eq. 9, listed in Table S1). Using these expressions, we can calculate the force due to the lateral surface $s1$ (Eq. 7). We use similar ideas to calculate the force on a given node due to the basal surface. We add the contributions from neighboring lateral and basal surfaces to find the net force on the vertex $\mathbf{r}_i$.

Area terms	$\partial/\partial x_i$	$\partial/\partial y_i$	$\partial/\partial z_i$
$2A^x_1$	0	$(z_{i-1} - z_c) + \frac{1}{n}(z_i - z_{i-1})$	$-(y_{i-1} - y_c) - \frac{1}{n}(y_i - y_{i-1})$
$2A^y_1$	$-(z_{i-1} - z_c) - \frac{1}{n}(z_i - z_{i-1})$	0	$(x_{i-1} - x_c) + \frac{1}{n}(x_i - x_{i-1})$
$2A^z_1$	$(y_{i-1} - y_c) + \frac{1}{n}(y_i - y_{i-1})$	$-(x_{i-1} - x_c) - \frac{1}{n}(x_i - x_{i-1})$	0
$2A^x_2$	0	$-(z_{i+1} - z_c) - \frac{1}{n}(z_i - z_{i+1})$	$(y_{i+1} - y_c) + \frac{1}{n}(y_i - y_{i+1})$
$2A^y_2$	$(z_{i+1} - z_c) + \frac{1}{n}(z_i - z_{i+1})$	0	$-(x_{i+1} - x_c) - \frac{1}{n}(x_i - x_{i+1})$
$2A^z_2$	$-(y_{i+1} - y_c) - \frac{1}{n}(y_i - y_{i+1})$	$(x_{i+1} - x_c) + \frac{1}{n}(x_i - x_{i+1})$	0
$2A^x_j$	0	$\frac{1}{n}(z_j - z_{j-1})$	$-\frac{1}{n}(y_j - y_{j-1})$
$2A^y_j$	$-\frac{1}{n}(z_j - z_{j-1})$	0	$\frac{1}{n}(x_j - x_{j-1})$
$2A^z_j$	$\frac{1}{n}(y_j - y_{j-1})$	$-\frac{1}{n}(x_j - x_{j-1})$	0

Table S1: Expressions for derivatives of surface area terms involved in calculation of force terms (Eq. 9). n is the number of vertices in a surface and the surface centroid is denoted by $\mathbf{C}_{s1} = x_c\hat{\mathbf{i}} + y_c\hat{\mathbf{j}} + z_c\hat{\mathbf{k}}$. See S1.2 for more details.

We use a similar approach to find the cell volume incompressibility force term. There are three neighboring cells for vertex $\mathbf{r}_i$. For one cell $v1$ containing vertex $\mathbf{r}_i$, we calculate the derivative in the following way

$$E_{v1} = B(V_{v1} - V_0)^2,$$

$$\mathbf{F}_{v1} = \nabla_i E_v = 2B(V_{v1} - V_0)\nabla_i V_{v1},$$

$$\nabla_i V_{v1} = \sum_{j=0}^{n_s-1} \nabla_i V_j,$$

$$\frac{\partial V_j}{\partial x_i} = \frac{1}{3}\sum_{i=0}^{n-1}\left(\left(\frac{\partial A_i^x}{\partial x_i}\hat{\mathbf{i}} + \frac{\partial A_i^y}{\partial x_i}\hat{\mathbf{j}} + \frac{\partial A_i^z}{\partial x_i}\hat{\mathbf{k}}\right)\cdot \mathbf{C}_j + \frac{1}{n}A_i^x\right),$$

$$\frac{\partial V_j}{\partial y_i} = \frac{1}{3}\sum_{i=0}^{n-1}\left(\left(\frac{\partial A_i^x}{\partial y_i}\hat{\mathbf{i}} + \frac{\partial A_i^y}{\partial y_i}\hat{\mathbf{j}} + \frac{\partial A_i^z}{\partial y_i}\hat{\mathbf{k}}\right)\cdot \mathbf{C}_j + \frac{1}{n}A_i^y\right),$$

$$\frac{\partial V_j}{\partial z_i} = \frac{1}{3}\sum_{i=0}^{n-1}\left(\left(\frac{\partial A_i^x}{\partial z_i}\hat{\mathbf{i}} + \frac{\partial A_i^y}{\partial z_i}\hat{\mathbf{j}} + \frac{\partial A_i^z}{\partial z_i}\hat{\mathbf{k}}\right)\cdot \mathbf{C}_j + \frac{1}{n}A_i^z\right).$$

We already have the expressions for the surface area derivative terms (Table S1) needed to calculate the cell volume incompressibility force term. The approach is extended to find the expression for force corresponding to the internal fluid and to the outer membrane term.

S2: Modifications to the naturally planar 2D vertex model
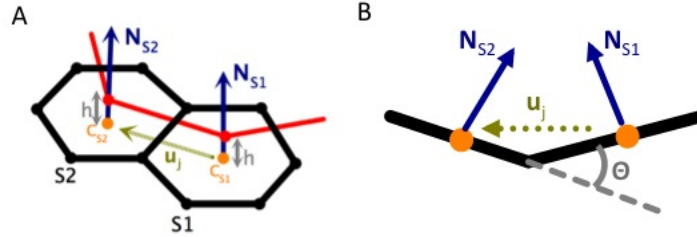

Figure S2: 2D vertex model. **(A)** Schematic to explain *offset* contractile segment (shown in red) in the 2D vertex model. The figure shows two adjacent cells $S1$ and $S2$ with shared edge j, centers $(\mathbf{C}_{S1}, \mathbf{C}_{S2})$ and unit normals $(\mathbf{N}_{S1}, \mathbf{N}_{S2})$. $\mathbf{u}_j$ is the unit vector joining the cell centers. The red line highlights a contractile segment joining the cell centers that is offset by a distance h from the surface along the cell normals. **(B)** Schematic of the configuration shown in (A) as viewed in the plane perpendicular to the common edge. Here, for the sake of illustration, we are assuming that each of the surface is planar or very close to planar.

S2.1 : Bending energy term with natural curvature

The naturally planar 2D vertex model has a bending energy term which corresponds to a naturally flat sheet. We modify it to represent natural curvature of the sheet in the following way

$$E_{bend} = \beta \sum_{j'} \left((1 - \mathbf{N}_{S2(j')} \cdot \mathbf{N}_{S1(j')}) - k_{j'}(-(\mathbf{N}_{S2(j')} - \mathbf{N}_{S1(j')}) \cdot \mathbf{u}_{j'} \right). \tag{10}$$

The modified bending energy term defines an equilibrium value of the angle between the adjacent normals of the interior edges. We define the normal of the cell S in the following way

$$\mathbf{N}_S = \frac{\mathbf{A}_S}{|\mathbf{A}_S|},$$

$$\mathbf{A}_S = \frac{1}{2} \sum_{i=0}^{n_s-1} (\mathbf{r}_i \times \mathbf{r}_{i+1}),$$

where n_s is the number of vertices of the cell S. List of vertices are ordered in each cell such that the normal vector points 'outside' the shell (Fig. S2, for further detail about the implementation of the 2D model refer to (3)).

Consider the two cells $S1$ and $S2$ adjacent to a particular interior edge j' (Fig. S2). Suppose that the normals $\mathbf{N}_{S1}$ and $\mathbf{N}_{S2}$ stay coplanar with the unit vector $\mathbf{u}_j$, as depicted in Fig. S2(B). Let θ be the angle between the normals $\mathbf{N}_{S1}$ and $\mathbf{N}_{S2}$) and assume that the unit vector $\mathbf{u}_j$ is perpendicular to the average normal $i.e.$ $\mathbf{N}_{S1}$ and $\mathbf{N}_{S2}$ make an angle $(\pi - \theta)/2$ and $(\pi + \theta)/2$ with $\mathbf{u}_j$, respectively. In the modified bending energy term (eq. 10), the contribution coming from this segment is proportional to

$$1 - \cos\theta - k_{j'}(-2\sin(\theta/2)). \tag{11}$$

The new term in the bending energy defines a rest value (i.e when the configuration is at equilibrium) of the angle between adjacent normals . This implements the notion of natural curvature precisely. Indeed, minimization of the bending energy in equation above with respect to theta yields the rest value θ_{eq} of the angle θ as a function of $k_{j'}$. In the particular case $|\theta| \ll 1$, the bending energy contribution can be approxiamted as

$$\frac{\theta^2}{2} + k_{j'}\theta \approx \frac{(\theta + k_{j'})^2}{2} - \frac{k_{j'}}{2}, \tag{12}$$

and the rest value of the angle between adjacent normals is given by $\theta_{eq} = -k_{j'}$.

If $k_{j'}$ is constant for all segments, the shell has homogeneous natural curvature. If $k_{j'} = 0$, bending energy corresponds to a naturally flat sheet. For the homogeneous shell configuration analysis, we set $k_{j'}$ as l_c/R for all the edges where R is the radius of the initial spherical configuration and l_c is the approximate average distance between the cell centers ($l_c = 2\bar{a}\cos(\frac{\pi}{6})$ where $\bar{a}$ is the average edge length of the polygonal cells). As an example, for the parameters listed in Table S4 (with $k_{j'} = 0.19$), the angle between normals for the adjacent cells for the closed shell homogeneous equilibrium configuration (i.e. with no prepatterning) is $\theta = 0.19 \pm 0.02$, which is very close to the value of $k_{j'}$.

S2.2: Offset contractile segments

In the new implementation, contractile segments are introduced along the cell centers and the additional energy of the prepatterning is defined as E_Γ (main text Eq. 5). E_Γ is the linear truncation of $\tilde{E}_\Gamma$. We define $\tilde{E}_\Gamma$ in the following way,

$$\tilde{E}_\Gamma = \Gamma \sum_{j=1}^{n} (|(\mathbf{C}_{S1(j)} + h\mathbf{N}_{S1(j)}) - (\mathbf{C}_{S2(j)} + h\mathbf{N}_{S2(j)})|). \tag{13}$$

Essentially, the offset contractile segments are the edges joining the points $(\mathbf{C}_{S(j)} + h\mathbf{N}_{S(j)})$. The vertices of this segment are obtained by offsetting the cell centers using the normals with an offset length h (Fig. S2). This term does two things: it applies a line tension that tries to bring the cell centers close together; additionally, when $h \neq 0$, it tries to bend the surface so that the endpoints of the normal vectors move closer together ($h > 0$) or further apart ($h < 0$), in such a way that the offset segment is as short as possible. The second effect changes the rest angle between the normals of the cells joined by the contractile segment. This term is similar to that of the modified bending energy term (Eq. 9), as both induce a local change in the natural curvature of the shell.

S3: Initial configuration, continuation, and symmetry

In the main text, we discussed the construction of the initial configuration and the numerical methods we used to find the equilibrium configuration. Here, we give further details about the numerical aspects of the implementation, particularly on the role of the inherent translational and rotational symmetry of the system.

Using the approach described in Section S6.1, we obtain the parameter values for which a shell made up of identical ideal cells are at equilibrium. Then, we use DistMesh (1), a meshing package that gives a triangular tessellation of a given edge length, to build a mesh on the sphere that is close to an ideal case configuration. We use the dual mesh, which is made up of the centers of the triangular elements, to construct polygonal cells. This forms the initial configuration for the 2D model and the inner surface of the epithelial shell for the 3D model. The vertices on the inner surface can then be extended radially to get an epithelial shell made up of 3D cells with distinct top and bottom surfaces. Here, we want to emphasize that not all apical and basal surfaces are hexagons in our initial spherical configuration - some are pentagons and heptagons. For example, in the case of a 2D initial spherical configuration with edge length = 0.55 and radius = 5.0, we have 346 hexagons, 40 pentagons and 28 heptagons after meshing. Although configurations built using the meshing package differ slightly from the ideal cases, where all cells should have same morphology, they still provide a good initial guess for finding the homogeneous equilibrium configuration, which then serves as the initial point for the prepatterning analysis.

To implement the Newton-Raphson method and pseudo-arclength continuation, we approximate the derivatives of the forcing function *i.e.* the Jacobian (or equivalently the Hessian matrix in this case) by the first order forward finite-difference method (one could

also use automatic differentiation). This complete Jacobian has six zero eigenvalues at a steady state for systems with rotational and translational symmetry, for example a closed shell in the absence of the outer shell term. We "pin" an appropriate number of vertices to make the Jacobian non-singular and to remove neutral stability directions (*i.e.* translationally and rotationally invariant solutions). We fix the coordinates of one vertex to be the origin, restrict the motion of a second vertex to only the radial direction, and restrict that of a third vertex to the radial and azimuthal directions to account for the six degrees of freedom. In the presence of the outer shell term, the system has only rotational symmetry, and pinning of a vertex is relaxed in such cases.

S4: Parameters used in simulations

Figure 2 : apical-in configuration	$\alpha = 2.13, \gamma = 0.98, \sigma = 1, B = 100, B_Y = 0, \epsilon = 10^{-10}, R_c = 6.025, n = 4$	$N_c = 414, \overline{a_A} = 0.55, h = 1.0, R_A = 5$
Figure 3 : apical-out configuration	$\alpha = 1.89, \gamma = 0.94, \sigma = 1, B = 100, B_Y = 0, \epsilon = 10^{-10}, R_c = 6.025, n = 4$	$N_c = 414, \overline{a_B} = 0.55, h = 1.0, R_B = 5$

Table S2: Parameter values used for simulations for the 3D vertex model (main text Fig. 2 and 3), where N_c is the total number of cells, $\overline{a_A}$ is the average length of apical edges, h is the height of cells, $\overline{a_B}$ is the average length of basal edges, R_A is the radius of the initial spherical configuration that makes the apical surface for the *apical-in* case, and R_B is the radius of the initial spherical configuration that makes the basal surface for the *apical-out* case. Other parameters are defined in main text.

Figure 4 : embedded contractile ring in a closed shell configuration	$\mu = 2.26, \sigma = 1, \beta = 0.005, B_Y = 0, \epsilon = 10^{-10}, R_c = 5.025, n = 4$	$N_c = 414, \overline{a} = 0.55, R_0 = 5$

Table S3: Parameter values used for simulations for the naturally planar 2D vertex model (main text Fig. 4), where N_c is the total number of cells, a is the edge length of hexagons that constitute flat configurations, $\overline{a}$ is the average edge length of polygonal cells that constitute curved configurations, R_i is the radius of the curved configuration, and R_0 is the radius of the initial spherical configuration. Other parameters are defined in main text.

Figure 5 : apical-in case	$h = -1, \mu = 2.26, \sigma = 1, \beta = 0.02, k_{j'} = 0.19, B_Y = 0, \epsilon = 10^{-10}, R_c = 5.025, n = 4$	$N_c = 414, \bar{a} = 0.55, R_0 = 5$
Figure 6 : apical-out case	$h = 1, \mu = 2.26, \sigma = 1, \beta = 0.02, k_{j'} = 0.19, B_Y = 0, \epsilon = 10^{-10}, R_c = 5.025, n = 4$	$N_c = 414, \bar{a} = 0.55, R_0 = 5$

Table S4: Parameter values used for simulations for the modified 2D vertex model (main text Fig. 5 and 6). Initial spherical configuration is same as previous analysis with the naturally planar 2D vertex model (Table S3). $h, k_{j'}$ are defined in main text. Definition of other variables are similar to Table S2.
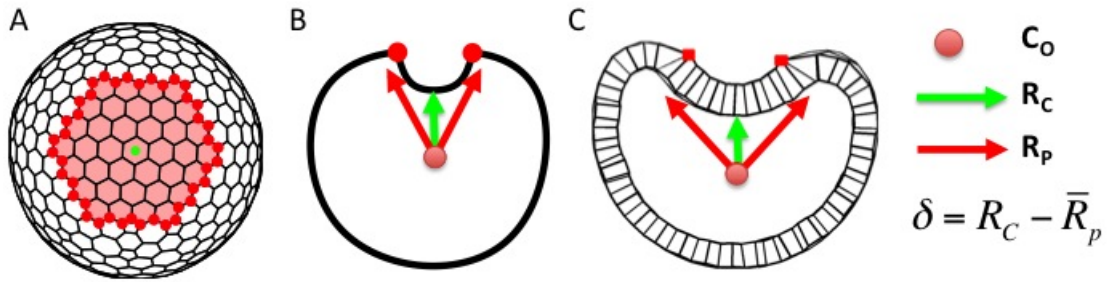
S5: Definition of δ

Figure S3: Defining δ to quantify bending of an epithelial shell due to the prepatterning of the line tension. $\mathbf{C}_0$ is the center of the initial homogeneous configuration with no prepatterning ($\Gamma = 0$). We use it as a reference center to define radial distance of the vertices. **(A)** A configuration with a constricting patch prepattern, highlighting cell vertices on the patch boundary (shown with red dots) and center of the patch (shown with a green dot). **(B)** For the 2D vertex model, δ is defined as the difference between the radial distance, from C_0, of the center of the patch (R_c) and the average radial distance of the vertices on the patch boundary ($\overline{R_p}$). **(C)** For the 3D vertex model, δ is defined as the difference between the radial distance of the center of the patch (R_c) and the average radial distance of the vertices on the patch boundary ($\overline{R_p}$) for the inner surface of the shell.
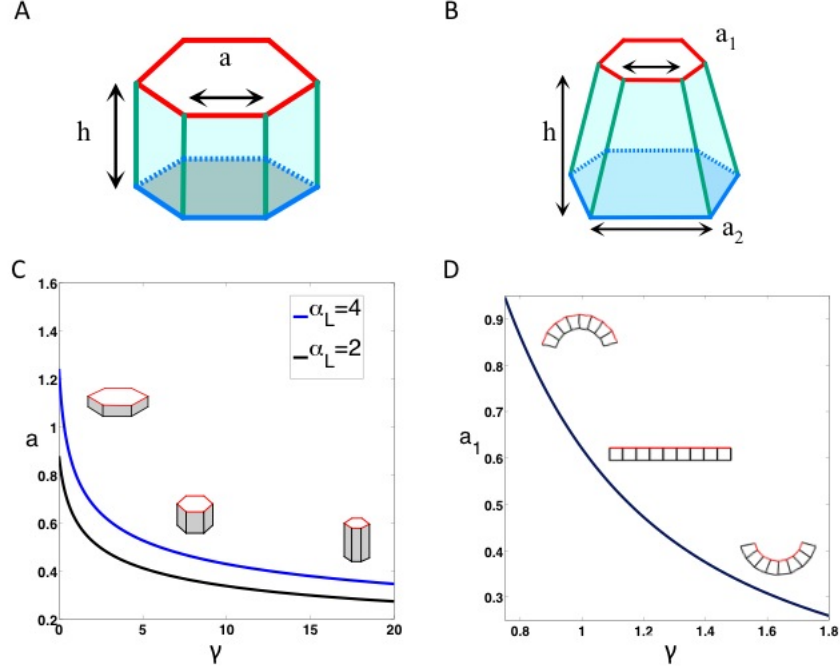
Figure S4: Cell shape as a function of model parameters for a hexagonal prism shaped and a lampshade shaped cell. **(A)** Hexagonal prism, part of a *flat* sheet, with height h and hexagonal edge a. **(B)** Lampshade-shaped prism, part of a *curved* sheet, with height h, apical edge a_1 and basal edge a_2. **(C)** The minimal energy states of a hexagonal prism shaped cell as a function of basal surface energy coefficient γ for a given lateral surface energy coefficient α. **(D)** The minimal energy states of a lampshade-shaped cell as a function of basal surface energy coefficient γ for a fixed basal edge length a_2. Schematics of the minimum energy configurations are shown as insets.

S6: Effect of model parameters

S6.1: Stable homogeneous configuration for the 3D vertex model

To obtain a good guess for the geometric and material properties for a stable homogeneous shell, we minimize the energy of a single cell in ideal cases. We consider two cases: hexagonal prism-shaped and lampshade-shaped cells (Fig. S4(A,B)). Hexagonal prism-shaped cells build a flat sheet whereas lampshade-shaped cells build a curved sheet.

In the case of hexagonal prism-shaped cells, both the basal and apical surfaces are represented by equivalent hexagons with edge length a and height h. We can write the non-dimensionalized form of the energy for a single cell by scaling length by $V_0^{1/3}$ and energy by $\sigma_e V_0^{1/3}$. We obtain the following equation for a hexagonal prism-shaped cell with three re-scaled parameters (keeping similar nomenclature after renaming : $\frac{\alpha V_0^{1/3}}{\sigma} \equiv \alpha, \frac{\gamma V_0^{1/3}}{\sigma} \equiv$

$\gamma, \frac{BV_0^{5/3}}{\sigma} \equiv B$).

$$E_c = 3a + 3\alpha a h + \gamma \frac{3\sqrt{3}}{2} a^2 + B(\frac{3\sqrt{3}}{2} a^2 h - 1)^2 \tag{14}$$

If we take the cell volume compression modulus to be large ($B \to \infty$), we can assume that V_C (cell volume) remains similar to V_0 (initial cell volume). This assumption provides a relationship between two geometric variables of the hexagonal prism, a and h ($h = \frac{2}{3\sqrt{3}a^2}$). The non-dimensionalized energy equation for a single cell reduces to

$$E_c = 3a + 3\alpha \frac{2}{3\sqrt{3}a} + \gamma \frac{3\sqrt{3}}{2} a^2 \tag{15}$$

The minima of the energy function, ($\frac{dE_c}{da} = 0$, $\frac{d^2 E_c}{da^2} > 0$) give a relationship between the material properties (α, γ) and the geometric parameter (a) that we use to generate an initial flat homogeneous configuration (Fig. S4(C)).

For lampshade-shaped cells, the edge lengths of the apical hexagonal face a_1 and the basal hexagonal base a_2 are different ($V_c = \frac{\sqrt{3}}{2}(a_1^2 + a_2^2 + a_1 a_2)h$). Following the previous analysis, the reduced energy expression for a lampshade-shaped cell is given by the following expression

$$E_c = 3a_1 + 3\alpha \frac{a_1 + a_2}{\sqrt{3}(a_1^2 + a_2^2 + a_1 a_2)} + \gamma \frac{3\sqrt{3}}{2} a_2^2 \tag{16}$$

This is a two variable minimization problem. The minima of this function ($(\frac{\partial E_c}{\partial a_1} = 0, \frac{\partial E_c}{\partial a_2} = 0$ and positive definite Hessian matrix) give a relationship between the material properties and the geometric parameters for the stable homogeneous shell (Fig. S4(D)).

In Fig. S4(C,D), we plot stable states for a single cell (solution for the minimization problem) around parameter values that we have used for the numerical experiments. In the case of hexagonal prism-shaped cells, if we decrease γ at fixed α, cells become squamous (smaller h). For lampshade-shaped cells with fixed basal surface edge length ($a_2 = 0.5$), increasing γ inverts the curvature. Above the value of γ for which cells are flat ($a_1 = a_2$), the apical side becomes the *inside* of the shell ($a_1 > a_2$), while below that value of γ the apical side becomes the *outside* of the shell ($a_1 < a_2$). Hannezo et al. did a similar analysis for their 3D model (2).

S6.2: Effect of curvature on deformation - Naturally planar 2D vertex model

We introduced a contractile ring (shown with red edges in Fig. S5(A) where $\Gamma > 0$) in the flat (Fig. S5(A)) and curved (Fig. S5(B)) configurations. Similar to Murisic et al. (3), we observed a supercritical pitchfork bifurcation as we increased Γ for the flat configuration with fixed boundary vertices (Fig. S5(D)). For the slightly curved configuration, we found a typical imperfect pitchfork bifurcation. Solutions with a patch of cells deflecting outward (*evaginated* state) formed a continuous branch of steady states from an initially homogeneous configuration, whereas solutions with a patch of cells deflecting inward (*invaginated* state) formed an isolated branch (Fig. S5(D)). Parameter values used for the simulation are $\mu = 2.45, \sigma = 1, \beta = 0, N_C = 217$ and $\bar{a} = 0.55$.
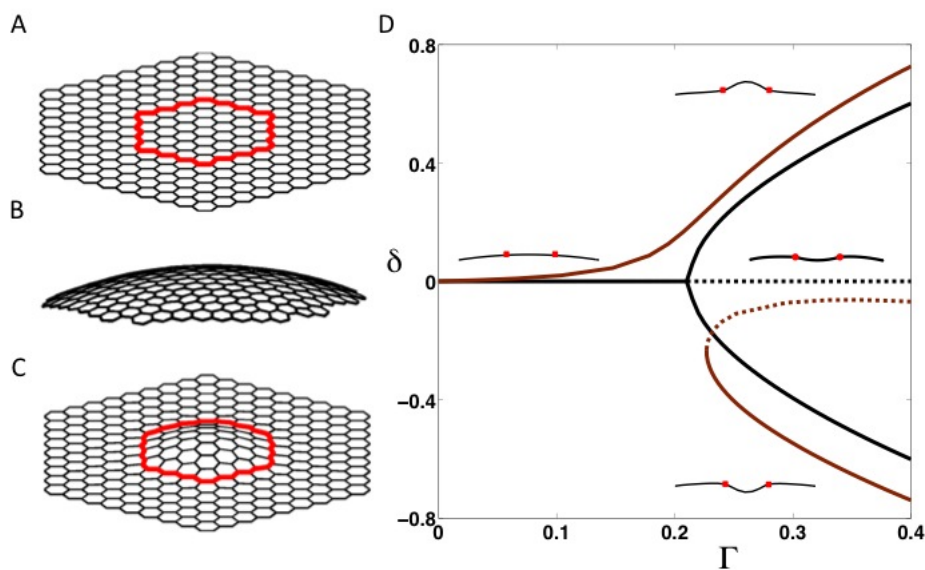

Figure S5: The effect of curvature on bending of the naturally planar 2D vertex model. **(A)** Flat homogeneous equilibrium configuration, showing a contractile ring prepattern. **(B)** Curved homogeneous configuration, which is a part of a shell (with radius $= 20$). **(C)** Representative equilibrium configuration for the flat configuration with $\Gamma > 0$ (where the enclosed patch is bending 'outward'). **(D)** Steady state diagram showing deflection δ with increasing parameter Γ for flat (black curve) and curved (brown curve) initial configuration. Solid (dashed) line:stable (unstable) steady states. Curvature results in an imperfect pitchfork bifurcation. Schematic cross-sections of representative states are shown as insets. Parameter values are listed in section S6.2.

S6.3: Effect of model parameters on deformations - Naturally planar 2D vertex model

We compared the equilibrium shapes of homogeneous shell ($\Gamma = 0$) in the presence and absence of the outer membrane term (Fig S6(A,B)). We found out that the outer membrane term kept the closed surface more spherical. We also assessed the effect of inner-fluid compression modulus (B_Y) and bending elasticity coefficient (β) for the naturally planar 2D vertex model. Increasing B_Y or β, while keeping the other parameters constant, increased the threshold after which invaginated states arises for the contractile ring prepatterning (Fig. S6(D,E)).

Figure S6: Effect of the outer membrane term and inner fluid incompressibility term on bending for the naturally planar 2D vertex model. **(A,B)** Initial homogeneous stable configuration: **(A)** In the presence of the outer membrane term ($\epsilon = 10^{-10}$); **(B)** In the absence of the outer membrane term ($\epsilon = 0$). The shape is more spherical in presence of the outer membrane term. Parameters used for the simulation are $\mu = 2.26, R_c = 5.025, n = 4, \sigma = 1, B_Y = 0, \beta = 0$ and the geometric parameters of the shell are same as main text analysis.**(C)** Steady state diagram showing deflection δ with increasing parameter Γ. Other parameters are as in **(A)**. Γ_{cr} is the limit point after which invaginated equilibrium shapes arises. **(D,E)** Region of bistability for the parameters: **(D)** bending elasticity coefficient (β) (for fixed $B_Y = 0.001$) and **(E)** Inner-fluid compression modulus (B_Y) (for fixed $\beta = 0$). Other parameters are same as (A).

S6.4: Effect of model parameters on deformations - 3D vertex model

We used the non-dimensionalized energy equation ($V_0 = 1, \sigma = 1$) for the following analysis. We kept $\alpha = 4$ fixed and the values of γ for which different aspect ratios of the homogeneous sheet (made up of hexagonal prisms) were at equilibrium and used them as the initial conditions. We considered three different cases here, $a = 0.5, \gamma = 5.96$, $a = 0.7, \gamma = 1.77$ and $a = 0.8, \gamma = 0.58$. Other parameters used were $\sigma = 1, B = 100$. We observed more deflection for the same force heterogeneity for thinner sheets, while the qualitative nature of the steady state diagram remains similar (Fig. S7).

We compared equilibrium shapes of homogeneous shell ($\Gamma = 0$) in the presence and absence of the outer membrane term for both cases: *apical-in* (Fig. S8(A-B)) and *apical-out* (Fig. S8(C-D)). Similar to the naturally planar 2D vertex model, we observed that the outer membrane term kept the closed surface more spherical. We also assessed the effect of inner-fluid compression modulus (B_Y) for both the *apical-in* (Fig. S9(C,D)) and *apical-out* (Fig. S9(A,B)) cases. If we increased B_Y, keeping other parameters constant, we saw a decrease in the deflection (Fig. S9).
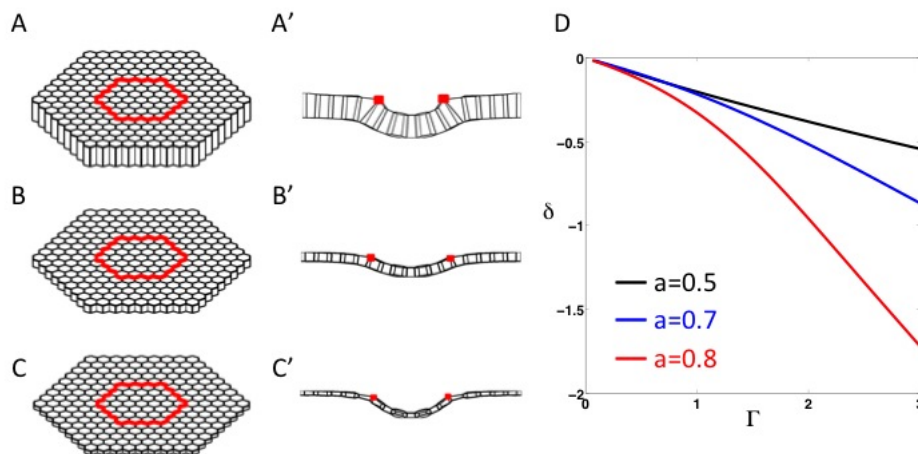

Figure S7: Effect of cell aspect ratio on bending for the 3D vertex model due to an apically embedded contractile ring. **(A-C)** Initial configurations with edge length 0.5, 0.7 and 0.8, respectively. Red edges $\Gamma > 0$; other edges $\Gamma = 0$. **(A'-C')** Cross-sections of invaginated steady states. **(D)** Steady state diagram showing deflection δ with increasing Γ. Parameter values are discussed in the Section S6.4.
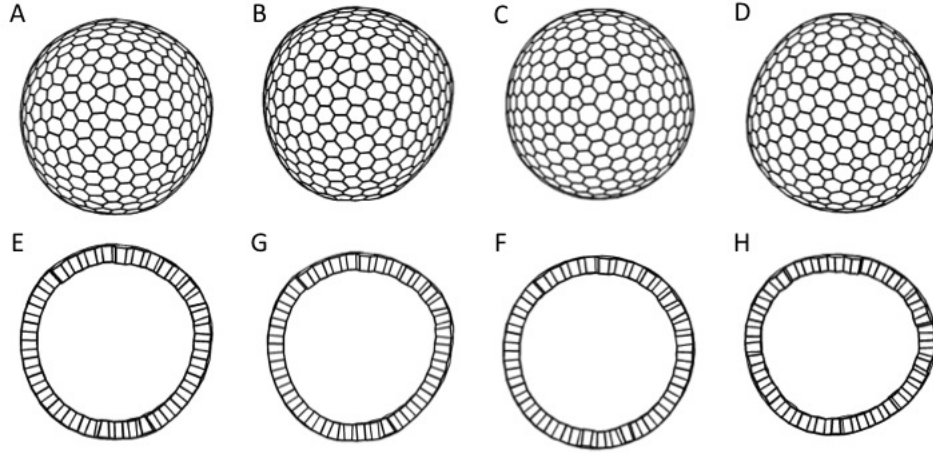
Figure S8: Effect of the outer membrane term for the 3D vertex model. **(A,B)** Initial homogeneous stable configuration for the *apical-in* case (see main text for details). **(A)** In the presence of the outer membrane term ($\epsilon = 10^{-10}$). **(B)** In the absence of the outer membrane term ($\epsilon = 0$).**(C,D)** Initial homogeneous stable configuration for the *apical-out* case (see main text for details). **(C)** In the presence of the outer membrane term ($\epsilon = 10^{-10}$) **(D)** In the absence of the outer membrane term ($\epsilon = 0$).**(E-H)** Cross-section of (A-D) respectively. The shape is more spherical in the presence of the outer membrane term in both cases. Parameter values used and geometry of the epithelial shell are the same as in the main text analysis (Table S2).
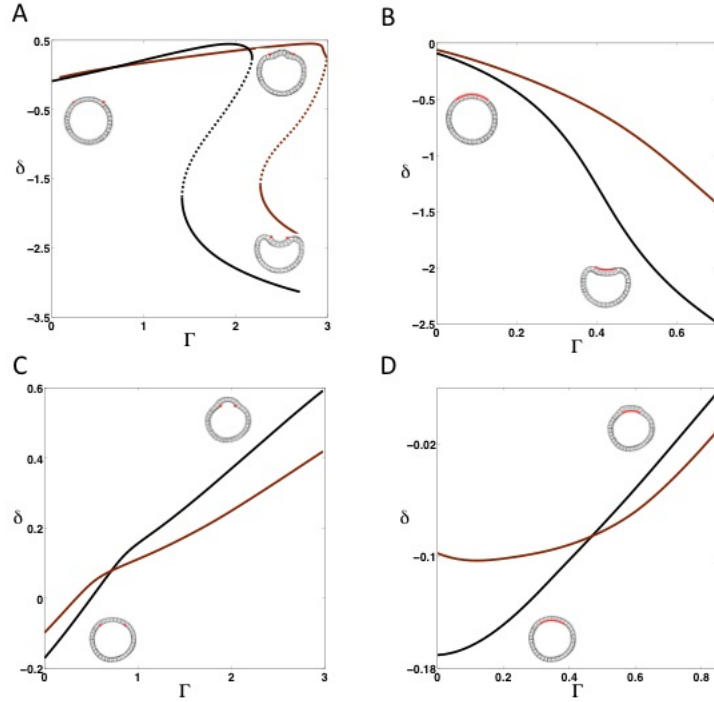
Figure S9: The effect of the inner fluid incompressibility term on deflection for the 3D vertex model. **(A-D)** Steady state diagrams showing deflection δ for different heterogeneities. **(A)** Contractile ring for the *apical-out* case. **(B)** Patch of apically constricting cells for the *apical-out* case. **(C)** Contractile ring for the *apical-in* case. **(D)** Patch of apically constricting cells for the *apical-in* case. Black curve: $B_Y = 0$; Brown curve: $B_Y = 0.001$. Solid (dashed) line: stable (unstable) steady states. Schematic cross-sections of representative states are shown as insets. Deflection is typically less for increased inner-fluid compression modulus. Parameter values used and geometry of the epithelial shell are same as main text analysis (Table S2).

S6.5: Effect of model parameters on deformations - 2D vertex model

Similar to the 3D vertex model, we observed that increasing inner-fluid compression modulus B_Y, while keeping other parameters constant, caused a decrease in the deflection for both *apical-in* and *apical-out* case (Fig. S10).
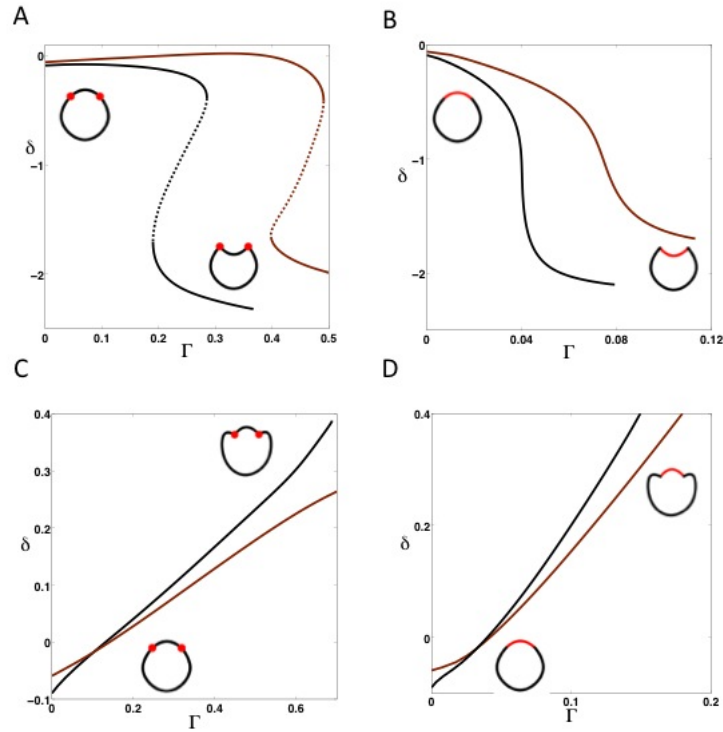

Figure S10: The effect of the inner fluid incompressibility term on bending for the 2D vertex model. **(A-D)** Steady state diagrams showing deflection δ for different heterogeneities. **(A)** Contractile ring for the *apical-out* case. **(B)** Patch of constricting cells for the *apical-out* case. **(C)** Contractile ring patterning for the *apical-in* case. **(D)** Patch of constricting cells for the *apical-in* case. Black curve: $B_Y = 0$; Brown curve: $B_Y = 0.001$. Solid (dashed) line: stable (unstable) steady states. Schematic cross-sections of representative states are shown as insets. Deflection is less for increased inner-fluid compression modulus. Parameter values used and geometry of the epithelial shell are same as main text analysis (Table S4).
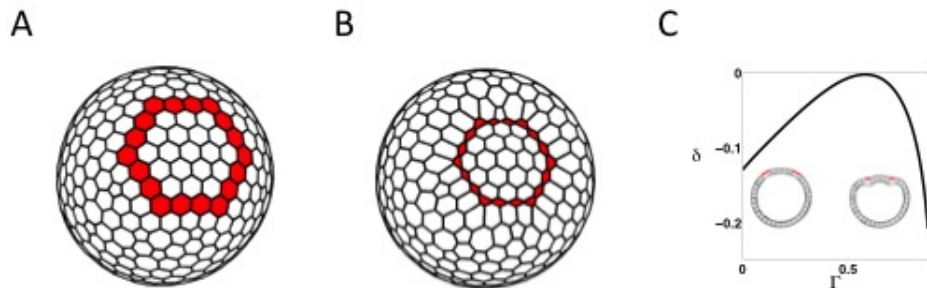
Figure S11: 3D deformations induced by a ring of apically constricting cells, one-cell wide, with 3D cells for the *apical-out* case. **(A)** Initial configuration showing the outer surface (i.e. apical side) of the shell. **(B)** Representative invaginated state. **(C)** Steady state diagram showing deflection δ with increasing parameter Γ. Cross-sections of representative steady states (A,B) are shown as insets. Parameter values are listed in Table S2 (simialr to Fig. 3 in main text).

S6.6: Effect of curvature on deformations - 3D vertex model

We analyzed the effect of prepatterning and curvature on the equilibrium shapes of epithelial shells made up of 3D cells. We considered shells of four different curvatures C (= inverse of the radius of spherical shells from which the system is initialized, Fig. S11(A)). We used epithelial cells with the following geometric and model parameters for all cases discussed here: $a_B = 0.55, h = 1.0, \gamma = 0.95, \alpha = 1.9, \sigma = 1$. The approximate nature of meshing on the spherical surface caused the number of cells (210 ± 10) and the basal edge length ($a_{basal} = 0.55 \pm 0.01$) to be slightly different for different shell configurations (see Materials and Methods section for details). We kept the boundaries of the shells fixed for both apical and basal surfaces.

We found a single continuous branch of stable steady states for apical constriction of a patch of cells. In this case, deflection monotonically increases with increasing Γ (Fig. S11(G)). On the other hand, we observed bistability in the shapes of shells for the contractile ring prepattern in shells above a certain curvature (Fig. S11(H)). There were two stable shapes for the same value of Γ, one with a slightly evaginating patch of cells (deflecting outward) and one with an invaginating patch of cells (delfecting inward). The upper limit point in the branch of steady states defined a threshold for the heterogeneity parameter, after which we observed a sudden bending of the sheet.
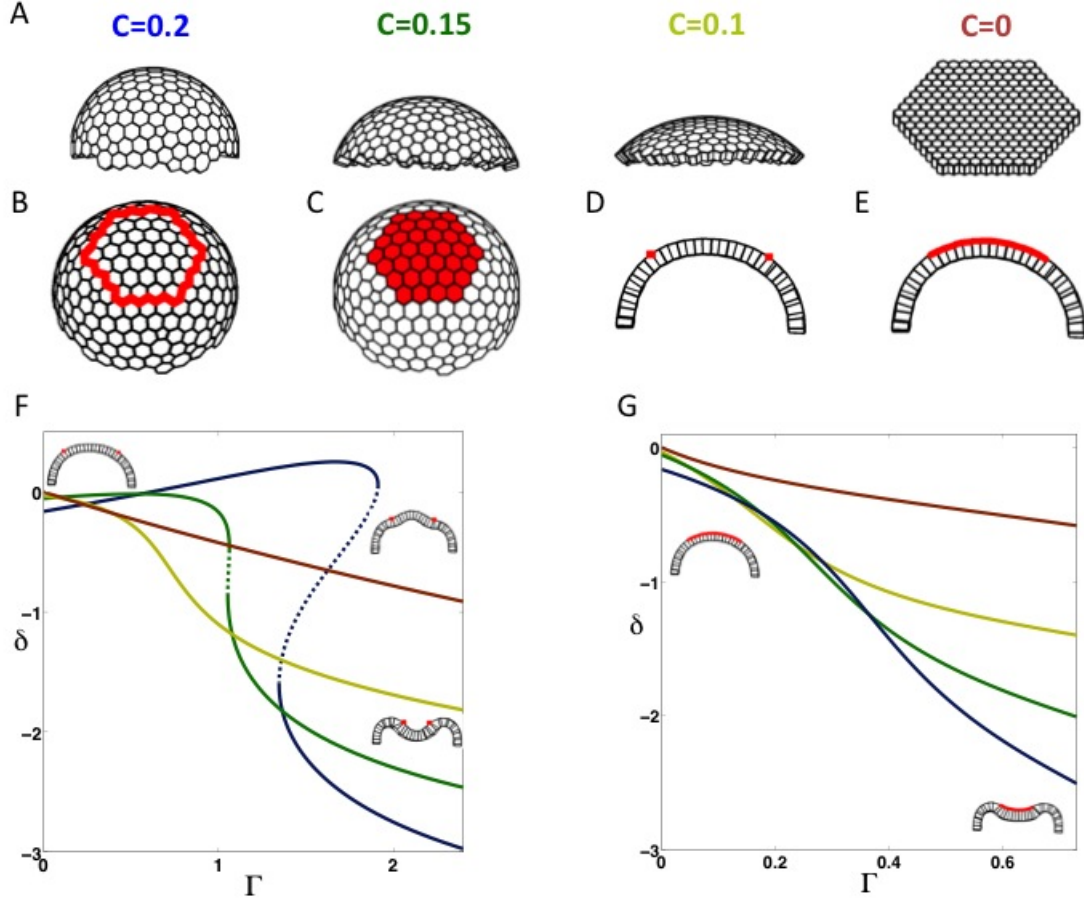
Figure S12: The effect of curvature on bending for the 3D vertex model. **(A)** Four different initial configurations with curvatures $C = 0.2, 0.15, 0.1$, and 0, respectively. **(B)** Contractile ring heterogeneity, highlighted on the initial configuration with C=0.2. The number of cells enclosed by the cable or included in the patch were similar for all initial curvatures. **(D,E)** Cross-sections of B and C respectively. **(F-G)** Steady state diagram showing deflection δ with increasing parameter Γ. Solid (dashed) line: stable (unstable) steady states. Color-coding of curves according to initial configuration matches color coding in A. Cross sections of representative steady states are shown as insets. Paramter values are listed in Section S6.6.

Supporting References

1. Persson, P. O., and G. Strang. 2004. A simple mesh generator in MATLAB. *SIAM Rev.* 46:329-345.

2. Hannezo, E., J. Prost, and J. F. Joanny. 2014. Theory of epithelial sheet morphology in three dimensions. *Proc. Natl. Acad. Sci. USA.* 111:27-32.

3. Murisic, N., V. Hakim, I. G. Kevrekidis, S. Y. Shvartsman, and B. Audoly. 2015. From Discrete to Continuum Models of Three-Dimensional Deformations in Epithelial Sheets. *Biophys. J.* 109:154-163.